British Journal of Applied Science & Technology
19(5): 1-8, 2017; Article no.BJAST.31798
ISSN: 2231-0843, NLM ID: 101664541

SCIENCEDOMAIN *international*
www.sciencedomain.org

Analysis of Reconfigurable Polarization Antenna as an EMI Sensor

Kumari Mamta[1*] and Raj Kumar Singh[2]

[1]Department of Applied Physics, Cambridge Institute of Technology, Ranchi, Jharkhand, India.
[2]Department of Physics, RLSY College, Ranchi University, Ranchi, Jharkhand, India.

Authors' contributions

This work was carried out in collaboration between both authors. Author KM designed the study, performed the statistical analysis, wrote the protocol and wrote the first draft of the manuscript. Authors KM and RKS managed the analyses of the study. Author KM managed the literature searches. Both authors read and approved the final manuscript.

Article Information

DOI: 10.9734/BJAST/2017/31798
Editor(s):
(1) Luigi Maxmilian Caligiuri, Faculty of Science, University of Calabria, Italy and Foundation of Physics Research Center (Director)- FoPRC, Italy.
Reviewers:
(1) Biswajeet Mukherjee, PDPM IIITDM, Jabalpur, India.
(2) Chung-Hsin Huang, Taipei College of Maritime Technology, Taiwan.
Complete Peer review History: http://www.sciencedomain.org/review-history/18313

Original Research Article

Received 25th January 2017
Accepted 7th March 2017
Published 23rd March 2017

ABSTRACT

Electromagnetic Interference (EMI) is of great concern in the present time of modern electronic systems. EMI measurement requires using a sensor to receive the radiation from the equipment in a suitable test environment. Antenna Factor decides the performance of the sensor. Finite Difference Time Domain (FDTD) numerical method has been used to predict the performance of antenna used as EMI sensor.

Keywords: Finite Difference Time Domain (FDTD); reconfigurable antenna; polarization; EMI; sensor.

1. INTRODUCTION

Recently, the polarization antenna has been attracting a lot of attention due to its unique features in enhancing the system performance, such as enhanced information content [1], frequency reuse [2], active tagging [3] as well as the improved capacity for multiple input multiple-out (MIMO) systems [4]. Because the polarizations are reconfigurable, the realization of

**Corresponding author: E-mail: mamta.singh548@gmail.com;*

compact size, economical, and low-profile capability becomes feasible. Typically, two effective solutions were utilized to generate the polarization reconfigurability. The first solution is to reconfigure the antenna's internal structure using switching components, such as PIN diodes and RF-MEMS switches [5]. Different resonant modes with diverse polarizations can be excited. By switching the PIN diodes along the antenna, both linear and circular polarization states can be achieved [6]. For a circularly polarized antenna, both mode of polarization i.e. the left-hand circular polarization (LHCP) and right-hand circular polarization (RHCP) can also be switched [7]. In addition, different linear polarization (LP) states can be formed by controlling the PIN diodes between the patch edges and ground [8]. Meanwhile, another popular solution is based on a tunable feeding network with multiple power routing schemes [9,10]. However, one has to manually switch between the two input ports, while the two varactors and a single-pole double-throw (SPDT) switch were employed for one-port design [10]. Based on a quasi-lumped coupler and a refined feeding system, one-port polarization-diversity antennas can also be realized [11,12]. But, they cannot provide the full polarization reconfigurability. Recently, a polarization diversity antenna with a compact feeding network was proposed [13]. It can supply full polarization states with only one-port input. The feeding network involves many lumped components, which result in the relatively high insertion losses (~ 2dB). Also, it requires a four-feed antenna, which could increase the complexity of the design process. Here reconfigurable polarization antenna as an EMI sensor is analyzed using FDTD method which has not been attempted as per the knowledge of the authors.

FDTD is one of the efficient numerical techniques to solve Maxwell's equations in any environments. For EMI measurement it is required to determine the field strength at the point of measurement using a sensor. To use the sensor for this purpose, calibration data is required relating the electric field at the aperture of the receiving antenna to the voltage at the 50Ω matched detector. Antenna Factor is the most common performance descriptor of EMI sensors. Antenna Factor [14] is defined as the ratio of the incident electric field on the surface of the sensor to the received voltage at the antenna terminal when terminated with a load. In this work the Finite Difference Time Domain (FDTD) technique has been used to evaluate the current distribution on the antenna surface when it is illuminated by the plane wave and subsequently calculate the voltage and hence Antenna Factor of the antenna.

Rest of the paper has been organized in the following order. Section II deals with antenna configuration. Followed by this in section III we discuss about antenna factor. Section IV focuses on cross polarization effect. Numerical analysis is given in section V. After numerical analysis we have included discussions in the next section. Finally, we conclude in section VII.

2. ANTENNA CONFIGURATION

The configuration of the proposed antenna is shown in Fig. 1. The antenna design process involves use of matlab and GID software.It is mainly composed of a radiating patch (square patch of side 61.34 mm) on a rectangular ground of dimension 180 mm x 120 mm, a 3 dB 90° hybrid coupler and Single Pole Double Throw (SPDT) switch. Vertex of the radiating patch labeled l_2 is at a distance of 70 mm from one end of the ground as shown in Fig. 1.

A Single Pole Double Throw switch (SPDT) is a single input switch that can connect to and switch between 2 outputs. A 3dB 90° hybrid coupler is a four port device used to equally split an input signal with a resultant 90° phase shift between output ports. It can also be used to combine two signals while maintaining high isolation between the ports.

The antenna substrate is 0.76 mm thick dielectric material with relative permittivity of $\varepsilon_r = 2.51$. The resonance frequency related to the length is 1.5175 GHz. In order to match the patch to the 50Ω lines of the coupler, two narrow 134. 2Ω lines with each length of 14.8mm have been introduced as impedance transformers. An impedance transformer is the one used to match the impedance. The 3 dB hybrid coupler is operated at 1.5175 GHz. Its four ports are shown in Fig. 1.

In Fig. 1, a FET SPDT switch is placed between the coupler and the input port of the antenna (denoted as P_0). Its insert loss and isolation are plotted in Fig. 2. When dc-bias voltages are V_2=3.5V and V_1 = 0 V, P_0 is connected with Port 1. The phase difference between Port 3 and Port 4 of the coupler is +90°. When dc-bias voltages are V_1=3.5V and V_2 = 0V, P_0 is connected with Port 2. The phase difference between Port 3 and

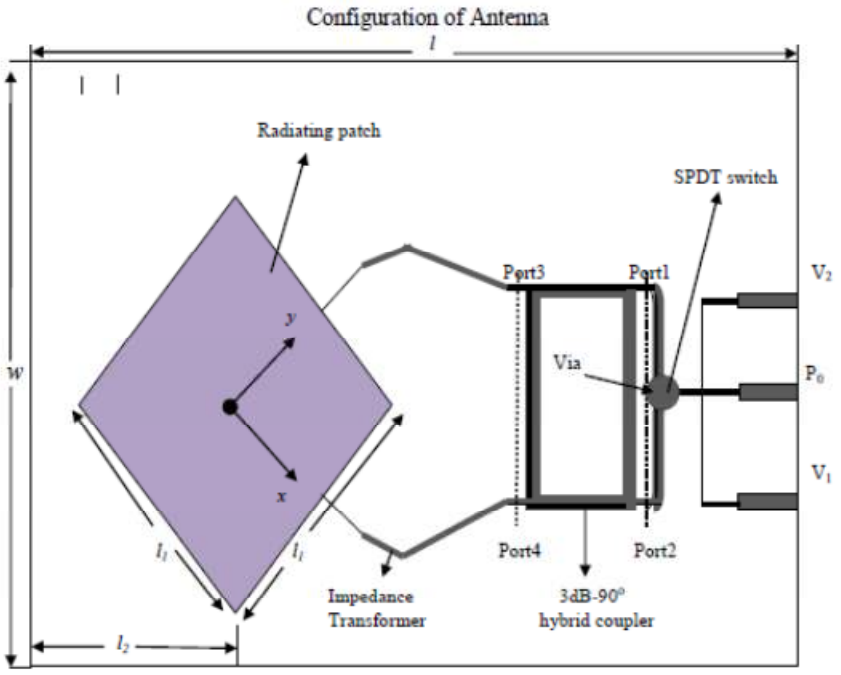

Fig. 1. Configuration of the microstrip patch antenna with a coordinate system. *l* = 180 mm, *w* = 120 mm, l_1 = 61.34 mm, l_2 = 70 mm

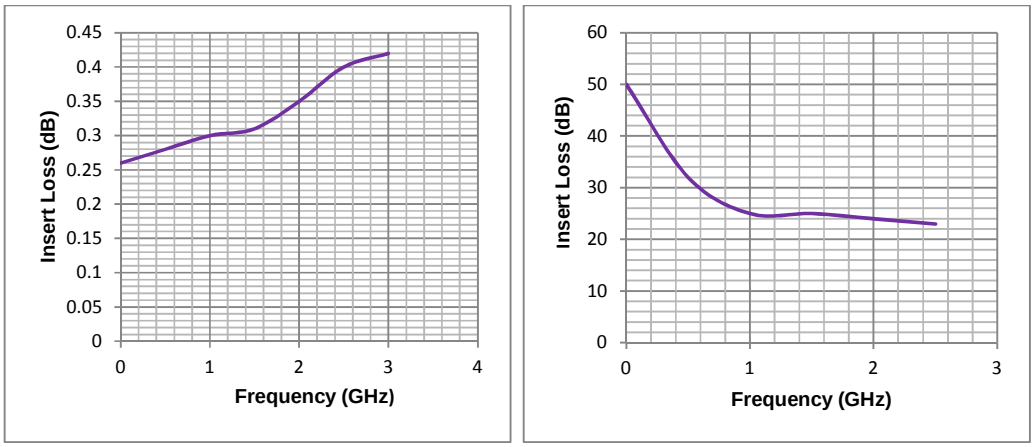

Fig. 2. Insert loss and isolation of single-pole double-throw switch

Port 4 is −90°. Therefore, the phase difference of two orthogonal modes for circular polarization can be switched between +90° and −90°.

3. ANTENNA FACTOR

The ratio of the incident electric field on the surface of the sensor to the received voltage at the antenna terminal when terminated by 50ohms load is known as Antenna Factor.

$$Antenna\ Factor = \frac{Incident\ Electric\ Field\ (E_i)}{\text{Re}ceived\ Voltage\quad (V)} \tag{1}$$

Thevenin's equivalent circuit diagram of an EMI sensor is shown in Fig. 3. The receiving antenna is replaced by an equivalent open circuit voltage at the two terminals of the antenna and its impedance. The open circuit voltage V_{oc} at the gap of the antenna is related to the incident electric field on the antenna surface.

The incident electric field E_i over each point on the antenna is uniform, whereas the impressed currents so produced on the wire are non-uniform. So to make an average, a crude approximation is made by introducing the effective length of the antenna, which when multiplied by the feeder current I_{sc}, equals to the integration of the impressed current over the length of the wire. Accordingly, the effective length is written as follows:

$$l_{effective} = \frac{\int_{-1/2}^{1/2} I.dl}{I_{sc}} \quad (2)$$

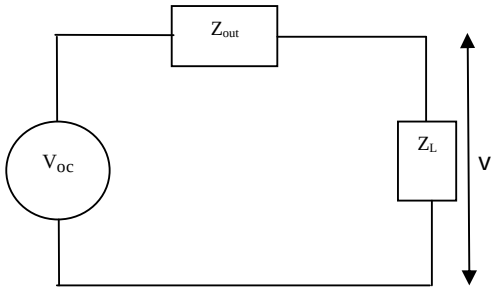

Fig. 3. Equivalent circuit diagram of a sensor

The open circuit voltage V_{oc} at the end terminals is written as follows:

$$V_{oc} = \vec{E}_i . \vec{l}_{effective} \quad (3)$$

The integral in equation (2) is approximated by the summation over N subsections.

$$l_{effective} = \frac{\sum_{n=1}^{N} I_n . \Delta_n}{I_{sc}} \quad (4)$$

The output impedance of the antenna is written as follows:

$$Z_{0ut} = \frac{V_{oc}}{I_{sc}} \quad (5)$$

From the equivalent circuit diagram the voltage to the receiver is achieved as follows:

$$V = \frac{Z_L}{Z_L + Z_{out}} V_{oc} \quad (6)$$

Generally Z_L i.e. impedance of the detector (e.g. spectrum analyzer) is considered as 50 ohms. To avoid the inaccuracy due to the approximations made in the evaluation of the open-circuited voltage in terms of the effective length of the antenna, the concept of the concentrated load is used later. In this method the load connected with the antenna is considered to be concentrated within the gap of the sensor.

In matrix solution the loaded antenna is considered to be divided into N number of segments each with constant current density. For a loaded antenna with J number of junctions each connecting M wire ends, the number of unknowns is reduced by $J\times (M-1)$. Enforcement of the boundary condition leads to $(N-J\times(m-1))$ number of equations are achieved with $(N-J\times(m-1))$ number of unknowns. This is transformed to matrix equation by applying the point matching technique as follows:

$$[V^i] = [Z][I]$$

Hence, above equation is modified as follows:

$$[V^i] = [Z'][I] \quad (7)$$

with $[Z'] = [Z] + [Z_C]$ where $[Z_C]$ is a diagonal matrix with only one non-zero diagonal element. Solving equation (7) following the same method, will give the current through the load, which when multiplied by the load will directly give the output voltage.

4. CROSS POLARIZATION EFFECT

Due to the presence of the LHCP and RHCP loading, loaded sensors are likely to suffer from cross polarization pick-up. Hence, while dealing with loaded antennas, the cross polarization characteristics of the antennas should be known. Here these studies have been performed in terms of the Antenna Factor of these antennas for the desired and cross-polarized electric field (Figs. 4a–4b).

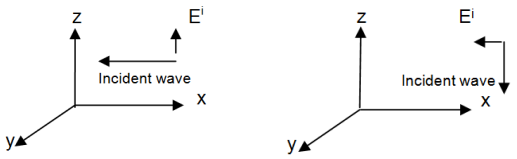

(a) **(b)**

Fig. 4. (a) Desired polarization and (b) Cross polarization of incident field

5. NUMERICAL ANALYSIS

The FDTD model uses a uniform space lattice cubic *Y* cells. Antenna (along *z*-axis) is illuminated by a *z*-directed linearly polarized plane wave. The time domain current *I*(*t*) flowing through the center of the antenna is calculated using Eqn.(8).

$$I\Big|^{n+1/2} = f_n \Delta x\left(H_x\Big|^{n+1/2}_{i_a, j_a-1, k_a+1} - H_x\Big|^{n+1/2}_{i_a, j_a, k_a+1}\right) + f_n \Delta y\left(H_x\Big|^{n+1/2}_{i_a, j_a, k_a+1} - H_x\Big|^{n+1/2}_{i_a-1, j_a, k_a+1}\right) \quad (8)$$

Where,

f_n is the normalized factor

During the progress of the FDTD calculations this field $E_z(t)$ and current $I(t)$ are saved for each time step. The FDTD calculations are continued until all transients are dissipated, so that the Fourier transform yields the steady-state frequency domain response of the antenna. Fourier transform of the current $I(t)$ gives frequency domain current $I(\omega)$ flowing through the center of the dipole. Voltage developed across 50Ω load is $V(\omega) = 50\ I(\omega)$. Finally antenna factor of the antenna is evaluated using Eqn. (1).

The fine spatial resolution permits direct modeling of the 0.4 cm radius wire, assumed to be PEC. A dipole of length 50 cm and radius 0.4 cm is illuminated by a plane wave of Gaussian impulse of maximum amplitude A = 1.0V/m given by the Eqn. (9) with t_0 = 0.26666 ns and t_ω = 0.08 ns. Antenna factor of the antenna is evaluated using Eqn. (1). Fig. 6 shows the phase part of the complex antenna factor of the antenna.

For Gaussian input pulse, the E_z component in the *abcd* plane at time step *t* is given by

$$E^t_{z_{i,j,k}} = Ae^{-0.5\left(\frac{t-t_o}{t_w}\right)^2} \quad (9)$$

6. DISCUSSION

The FDTD based virtual lab approach has several advantages over conventional measurement based methods for determining antenna factor.

- Antennas can be illuminated with a plane-electromagnetic wave. Time domain current and hence voltage across 50Ω load can be calculated. Single virtual lab gives all the frequency components of the results.
- Illumination by a single electromagnetic wave in the direction of bore sight is possible. Interactions between antennas and ground planes may be eliminated.

Measured values of Real and imaginary parts of input impedance show clear match with the theoretical values for different length of load arm to achieve resonance of inverted L-shaped antenna with main arm length of 0.3*λ*, radius equal to 0.004*λ* (Fig. 5). Fig. 6 shows the variation of phases of far field antenna with the frequencies. It is found that the phase of the far field antenna factor also fall in line with the expected values at different frequencies of the input signal. As shown in Fig. 3 phase is zero for

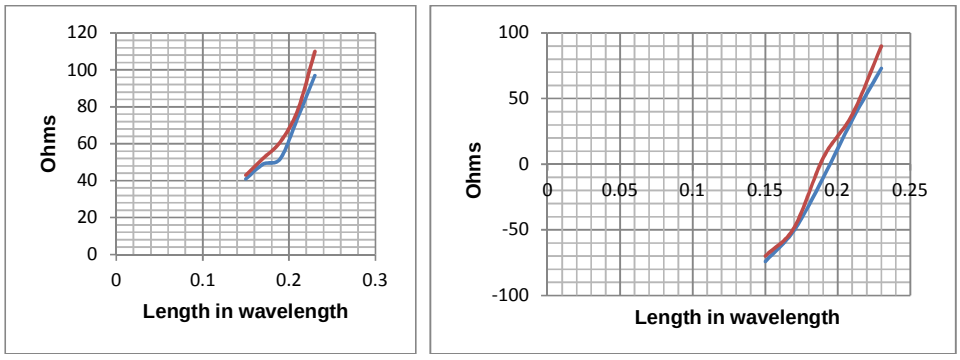

Fig. 5. Input impedance vs. length of load arm to achieve resonance of inverted L-shaped antenna with main arm length=0.3*λ*; radius=0.004*λ*. Top graph shows the plot of real part of impedance, IE 3D and theoretical results (blue and red line). Bottom graph shows the plot of imaginary part of impedance, IE 3D and theoretical results (blue and red line)

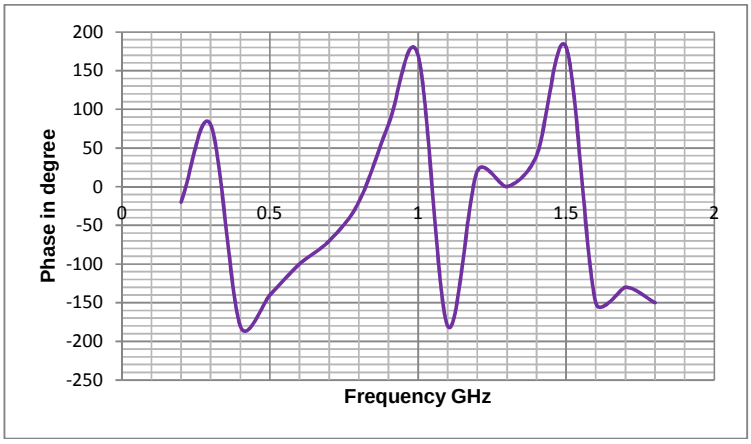

Fig. 6. Phase of the far field antenna factor

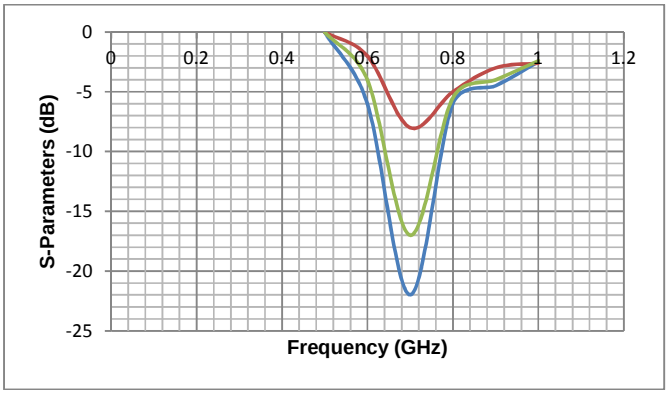

Fig. 7. S_{11} Parameter (in green colour). Measured value of parameter S_{11} for RHCP and LHCP (red and blue colour)

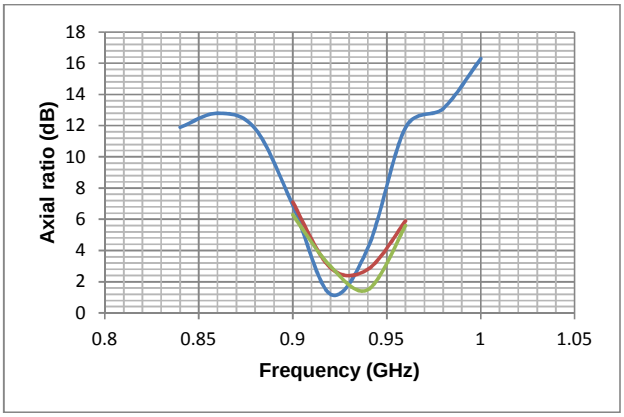

Fig. 8. Virtual lab and measured Axial Ratios (AR) of the polarization-agile antenna at State III (RHCP) and State IV (LHCP). Virtual lab AR in blue line. Measured ARs for RHCP and LHCP in red and green lines respectively

multi operating frequency. The polarization-agile antenna can operate at RHCP -or LHCP modes when the reconfigurable feeding network is switched between the States III and IV. The dependence of S_{11} parameter on the frequency of the input excitation is shown in Fig. 7. Virtual

lab result and the measured values of S-parameter S_{11} of the polarization agile antenna well agree for both the modes of RHCP and LHCP. It is important to note here that they show a resonance effect around 0.7 GHz frequency of the input excitation. Further, Axial ratios of the polarization agile antenna also agree well with the expected results. A resonance type behavior is observed in the virtual lab at 0.92 GHz, which is very close to the one for RHCP and LHCP (Fig. 8).

7. CONCLUSION

A reconfigurable antenna with high potentiality is proposed. The idea of this design is very simple. By using only one SPDT switch, the proposed antenna can be operated in left or right-hand circular polarization according to relatively simpler dc-bias voltage network. From the experimental results, the performances of the proposed antenna agree well in the LHCP and the RHCP case. It is very much suitable for wireless communication systems applications.

It is concluded that FDTD is very efficient, accurate and easy technique to compute the antenna factor of an antenna. We conclude from this work that the height of the sensors can be appreciably reduced by the introduction of the load arms without making any major compromise in the performance in terms of cross polarization isolation. Measured values of real and imaginary parts of input impedance show clear match with the theoretical values for different length of load arm to achieve resonance of inverted L-shaped antenna with main arm length of 0.3λ, radius equal to 0.004λ. Phase of the far field antenna factor also matches with the expected values at different frequencies of the input signal. Virtual lab result and the measured values of S-parameter S_{11} of the polarization agile antenna well agree for both the modes of RHCP and LHCP. It is important to note here that they show a resonance effect around 0.7 GHz frequency of the input excitation. Further, Axial ratios of the polarization agile antenna also agree well with the expected results. A resonance type behavior is observed in the virtual lab at 0.92 GHz, which is very close to the one for RHCP and LHCP.

However, it has been noticed that the radiation impedance of transmitting antenna and output impedance of receiving antenna are different.This is because the two cases are not reciprocal.

COMPETING INTERESTS

Authors have declared that no competing interests exist.

REFERENCES

1. Gao S, Sambell A, Zhong SS. Polarization-agile antennas. IEEE Antennas Propag. Mag. 2006;48(3):28–37.
2. Yang F, Rahmat-Samii Y. A reconfigurable patch antenna using switchable slots for circular polarization diversity. IEEE Microw Wireless Compon. Lett. 2002;12:96–98.
3. Kossel MA, Kung R, Benedickter H, Bachtold W. An active tagging system using circular polarization modulation. IEEE Trans. Microw. Theory Tech. 1999; 47(12):2242–2248.
4. Qin PY, Guo YJ, Liang CH. Effect of antenna polarization diversity on MIMO system capacity. IEEE Antennas Wireless Propag. Lett. 2010;9:1092–1095.
5. Simons R, Chun D, Katehi L. Polarization reconfigurable patch antenna using microelectromechanical systems (MEMS) actuators. Proc. IEEE AP-S Int. Antenna Propag. Symp. Digest. 2002;6–9.
6. Qin PY, Weily AR, Guo YJ, Liang CH. Polarization reconfigurable U-slot patch antenna. IEEE Trans. Antennas Propag. 2010;58(10):3383–3388.
7. Khidre A, Lee KF, Yang F, Elsherbeni AZ. Circular polarization reconfigurable wideband E-shaped patch antenna for wireless applications. IEEE Trans. Antennas Propag. 2013;61(2):960–964.
8. Qin PY, Guo YJ, Ding C. A dual-band polarization reconfigurable antenna for WLAN systems. IEEE Trans. Antennas Propag. 2013;61(11):5706–5713.
9. Row JS, Hou MJ. Design of polarization diversity patch antenna based on a compact reconfigurable feeding network. IEEE Trans. Antennas Propag. 2014; 62(10):5349–5352.
10. Mukherjee Iswajeet, Patel Pragati, Mukherjee Jayanti. A novel hemispherical dielectric resonator antenna with complementary split-ring-shaped slots and resonator for wideband and low cross-polar applications. IEEE Antennas and Propagation Magazine. 2015;57(1):120-128.

11. Wang K, Nelson R. Numerical virtual lab of the antenna factor of broad-band dipole antenna. IEEE International Symposium on EMC. 2001;1:616–619.
12. Row JS, Shih CJ. Polarization-diversity ring slot antenna with frequency agility. IEEE Trans. Antennas Propag. 2012;60(8): 3953–3957.
13. Tsai JF, Row JS. Reconfigurable square-ring microstrip antenna. IEEE Trans. Antennas Propag. 2013;61(5):2857–2860.
14. Paul CR, Introduction to electromagnetic compatibility, Wiley series in microwave and optical engineering. Wiley, New York; 1992.

Peer-review history:
The peer review history for this paper can be accessed here:
http://sciencedomain.org/review-history/18313